ELSEVIER

International Journal of Applied Earth Observation and Geoinformation 5 (2004) 219–237

INTERNATIONAL JOURNAL OF APPLIED EARTH OBSERVATION AND GEOINFORMATION

www.elsevier.com/locate/jag

Radiometric saturation of Landsat-7 ETM+ data over the Negev Desert (Israel): problems and solutions

Arnon Karnieli [a,*], Eyal Ben-Dor [b], Yunden Bayarjargal [a], Rachel Lugasi [b]

[a] *The Remote Sensing Laboratory, Jacob Blaustein Institute for Desert Research, Ben Gurion University of the Negev, Sede Boker Campus, 84990 Negev, Israel*

[b] *Department of Geography and Human Environment, Tel-Aviv University, Tel-Aviv, Israel*

Received 13 November 2003; received in revised form 6 April 2004; accepted 27 April 2004

Abstract

Unsuccessful efforts to interpret and analyze several sets of images acquired over Israel by Landsat-7 during the first 2 years of its operation (August 1999–August 2001) provided the motivation to examine the hypothesis that image data produced over the desert regions along the climatic transition zone of Israel were subject to radiometric saturation. The objectives of the current study are to characterize the saturation phenomenon, by inspecting different images of Landsat-7, and to suggest a statistic method for solution in the spectral domain. Entropy analysis was also performed on these images in order to compare the information content of the Landsat-7 Enhanced Thematic Mapper Plus (ETM+) sensor with that of the Landsat-5 Thematic Mapper (TM) over the desert environment before and after saturation correlation. The study reveals that radiometric saturation affected several ETM+ bands (especially band 3). Consequently, in terms of entropy, less information can be extracted from the saturated bands relative to equivalent bands of Landsat-5 TM. A statistical solution, based on multivariate correlation analysis among all spectral bands, is proposed to overcome the saturation problem. Satisfactory results were achieved by applying the statistical methods on several samples of saturated scenes. An operational revision in the spectral radiance range and the gain setting, applied to Landsat-7 ETM+ that is affected from July 1, 2000, has improved the saturation phenomenon over the region. The current proposed method can be applied for other climatic regions, such as scenes partially covered by snow, and other multi and hyper spectral sensors.

Keywords: Radiometric saturation; Landsat-7; Negev Desert; Entropy

1. Introduction

Landsat-7, which carries onboard the Enhanced Thematic Mapper Plus (ETM+) instrument, was launched on April 15, 1999 as part of the global research program of NASA's Earth Science Enterprise. This long-term program is aimed at understanding changes in the Earth's global environments including land, oceans, atmosphere, ice caps, as well as with life forms (Goward et al., 2001). The mission is accomplished through repetitive, synoptic coverage of continental surfaces. The sensor has six spectral bands in the visible, near-infrared, and shortwave infrared regions of the electromagnetic spectrum (at 30 m spatial resolution), one thermal infrared band (60 m and 120 m spatial resolution products), and one panchromatic band (at 15 m spatial resolution).

* Corresponding author. Tel.: +972 8 6596855; fax: +972 8 6596805.
E-mail address: karnieli@bgumail.bgu.ac.il (A. Karnieli).

0303-2434/$ – see front matter © 2004 Elsevier B.V. All rights reserved.
doi:10.1016/j.jag.2004.04.001

Absolute radiometric calibration to common units of measurement is an initial condition for a successful analysis of the Earth's surface by remote sensing. Data from several onboard devices are involved in the calibration processing. These devices are a new full-aperture-solar-calibrator and a partial-aperture-solar-calibrator that permit the use of the Sun as an absolute radiometric calibration source, since its exo-atmospheric irradiance is known. These data along with an internal calibration lamp and occasional ground-based validation experiments are expected to provide improved calibration accuracy within 5% (Thome, 2001; NASA, WWW1[1]).

Since images are acquired over different surface albedo, including dark water bodies, tropical forests, agricultural lands, bare soils, and very bright ice seas, it was necessary to design a sensor that covers the entire dynamic range that would accommodate this extensive surface brightness variety. Dynamic range is defined as the ratio of maximum measurable signal to minimum detectable signal (CCRS, WWW2). The lower limit is usually set by noise and the upper limit by saturation. Thus, a radiometric sensor is considered saturated when the input signal, in terms of voltage, exceeds the maximum measurable signal of the detector.

One of the improvements of the ETM+ instrument over the previous Thematic Mapper (TM) one, for enhancing radiometric precision, and consequently for better land-cover discrimination, is its capability to scan in either a low or highgain state. Gain is denoted as an increase in signal power during its transmission from one point to another in order to maximize the radiometric resolution (8 bits in the case of the ETM+) without saturating the detectors (whose digital number (DN) maximum is 255). The ETM+ is characterized by low gain dynamic range that is approximately 1.5 times greater than the high gain dynamic range. The gain attributes for the ETM+ were set such that for spectral bands 2, 3, 4, and 7, the low gain corresponds to the Landsat-5 8 bit gain attribute. Thus, when high gain is selected, the sensor acquires observations with greater radiometric sensitivity, until "saturation" is reached. For the other bands, 1 and 5, the high gain state replicates the Landsat-5 setting (Masek et al., 2001).

[1] URL addresses are listed in Appendix A.

Table 1
Gain setting rules for the land and desert surface cover categories

Band	Land	Desert
1	High	High for $H < 28^\circ$ Low for $H \geq 28^\circ$
2	High	High for $H < 28^\circ$ Low for $H \geq 28^\circ$
3	High	High for $H < 28^\circ$ Low for $H \geq 28^\circ$
4	High for $H < 45^\circ$ Low for $H \geq 45^\circ$	High for $H < 45^\circ$ Low for $H \geq 45^\circ$
5	High	High for $H < 38^\circ$ Low for $H \geq 38^\circ$
7	High	High for $H < 38^\circ$ Low for $H \geq 38^\circ$

H stands for sun elevation (compiled from NASA, WWW3).

Practically, the gain is switched by the Mission Operation Center (NASA, WWW3), for any specific scene, between low and high states as a function of the combination between the surface brightness and sun elevation. Consequently, brighter surfaces are scanned in the low gain mode and darker surfaces in the high gain mode (NASA, WWW3). Six Earth surface cover categories are involved in the gain setting operational rules, these are: (1) land (non-desert, no-ice); (2) desert; (3) ice/snow; (4) water; (5) sea ice; and (6) volcano/night. Since the current paper is dealing only with the first two categories, namely land and desert, their corresponding gain setting rules are presented in Table 1. From this table it can be noticed that, for the land category, only band 4 can be switched between high and low gains. The latter gain is set where the sun elevation is greater than 45° in order to avoid dense vegetation (reflectance > 0.66) saturation. At this sun angle, high gain in band 4 saturates at a reflectance of about 0.66. As such, switching to low gain prevents targets at this reflectance or below from saturating. Desert surfaces are relatively bright due to sparse vegetation (if any) as well as low water, organic, and iron oxides contents. Therefore, in the desert category low gains are set with respect to sun elevation to avoid bright desert target saturation when reflectances are higher than 0.66, 0.71, 0.65, 0.66, 0.70, and 0.68 in bands 1, 2, 3, 4, 5, and 7, respectively (NASA, WWW3).

Considerable efforts were involved in the pre-launch and post-launch calibration of the Landsat-7 ETM+ sensor using laboratory, on-board, and vicarious

(ground-based) methods (Thome et al., 1997). These efforts are aimed at achieving a reliable and quantitative use of the Landsat data in accordance with the mission goals specified above. Several recent publications have described and evaluated different calibration activities (Masek et al., 2001; Vogelmann et al., 2001; Teillet et al., 2001; Thome, 2001). None of them reports any severe problem with the sensor in terms of radiometric saturation except for one case, in which Thome (2001) briefly reports saturation in bands 3, 5, and 7, encountered during the vicarious calibration campaign that took place on July 20, 1999 in Roach Lake Playa (Nevada). No further difficulties were noticed from the other three campaigns conducted between June and October 1999 in Roach Lake Playa and the other desert sites.

Entropy has been applied as one of the methods to evaluate and compare the information content of different systems. Entropy was introduced by Shannon (1948) as a new probabilistic way of solving problems of efficiency in transmitting information over noisy communication channels. Mathematically, entropy (E) can be defined as:

$$E = -\sum_{i=0}^{N} p(i) \log_2 p(i) = -\frac{1}{\ln 2} \sum_{i=0}^{N} p(i) \ln p(i) \quad (1)$$

where $p(i)$ is the probability of occurrence of a DN between 0 and N (i.e., between 0 and 255 in Landsat's 8 bit system). Practically, the DN values are extracted from the scene's gray level histogram. Therefore, entropy is a measure for characterizing image signals. In a specific spectral band, $E = 0$ and $E = 8$ represent zero and maximum information content, respectively, in units of bits/pixel.

Price (1984) and Malila (1985) used entropy to compare the information contents of Landsat multispectral scanner system (MSS) and Landsat TM. Masek et al. (2001) applied the same method to compare between Landsat ETM+ and Landsat TM. In his study, Masek et al. first simulated DNs representing urban and forest environments for TM and ETM+. Later, they used actual TM and ETM+ data representing eight different environments, namely, estuarine water, residential area, growing crops, deciduous forest, urban, dry grassland, wetlands, as well as mixed environment. From that study Masek et al. showed that, in general, the information content of the ETM+ system is higher than that of the TM system in all bands except 1 and 5. Bands 2, 3, and 7 exhibited the highest additional information content (up to 1 bit) for most of the land-cover categories. Band 4 was more sensitive to vegetated areas. Bearing in mind that in bands 1 and 5 the high gain state nearly replicates the Landsat-5 setting, the results seem reasonable.

2. Objectives

Because of the unsuccessful efforts to interpret and analyze several sets of Landsat-7 images acquired over Israel during the first 2 years of the Landsat-7 operation (August 1999–August 2001) it was hypothesized that the desert regions along the transition zone of Israel are subject to radiometric saturation in the ETM+ sensor. The objectives of the current paper are to characterize the saturation phenomenon, to determine the extent of its occurrence by examining different images acquired since the start of operation of Landsat-7, and to suggest a methodology for partial solution. Another objective is to evaluate and to compare the information content of Landsat-5 and Landsat-7, before and after the saturation recovery.

3. Study area

Fig. 1 presents a mosaic image of Israel composed of three Landsat-7 ETM+ scenes, band 3, overlaid by mean annual rainfall isohyets for the last 50 years (data provided by the Climate Survey of Israel). Basically, Israel is a dryland that covers a 400 km cross-section of climatic zones from hyper-arid (25 mm mean annual rainfall in the south) to sub-humid (up to 900 mm in the north). The isohyetal belt between 200 and 300 mm is considered to be the desert boundary of Israel (Sofer, 1979). Precipitation occurs mainly during a short period of time, namely between November and April, while during May to September, the period is considered dry. In the Negev Desert, rainfall amounts decrease gradually from north to south with respect to the distance from the Mediterranean Sea. However, the Judean Desert lies in the rain shadow and is characterized by steep declining rainfall going towards the east. In mountainous areas, like in southern Israel, as the rising air masses become cooler, relative humidity

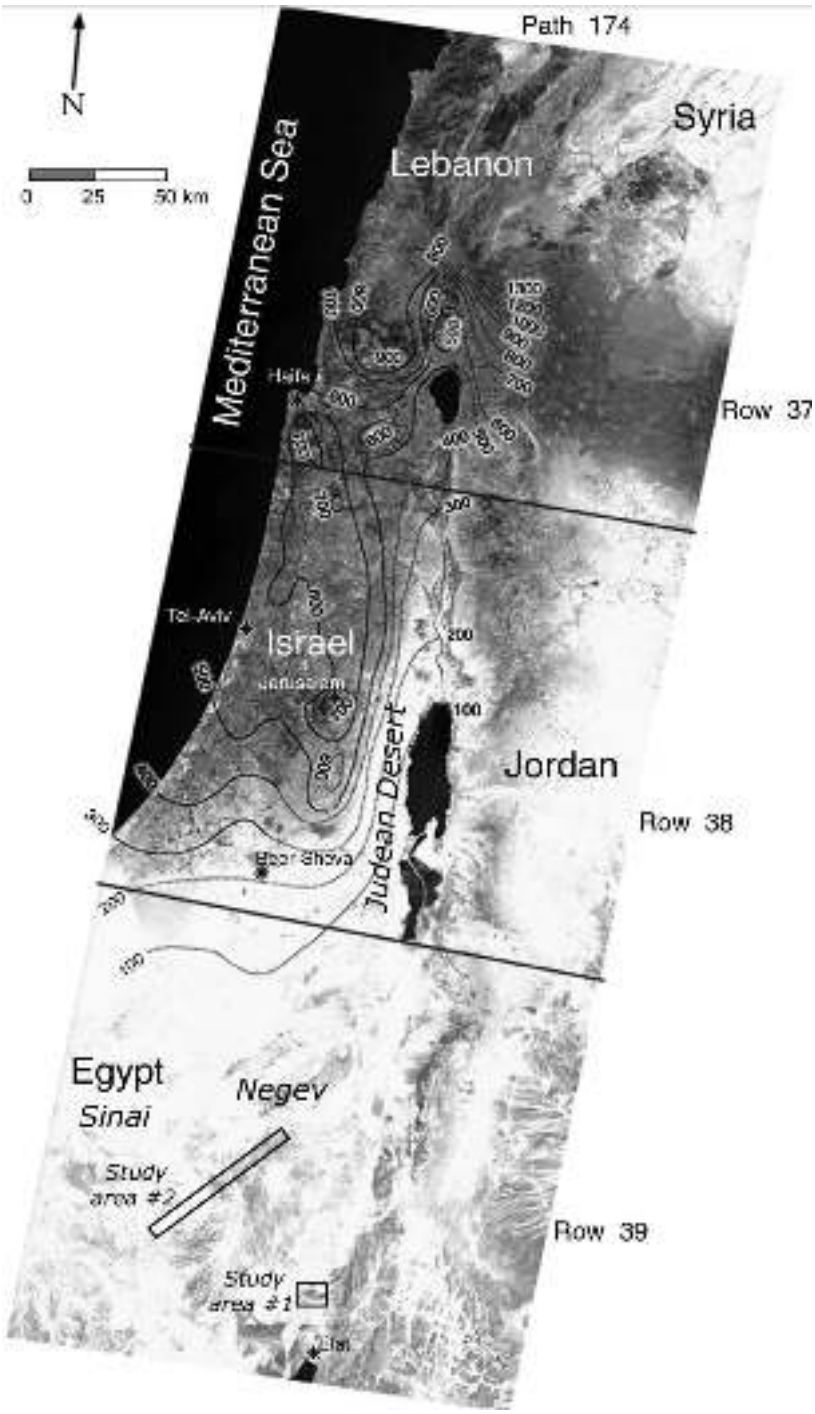

Fig. 1. Landsat-7 ETM+ scenes covering Israel (path/row = 174/37, 38, 39) overlaid with rainfall isohyets. Note the brightness contrast between the north and south sides of the 300 mm isohyetal line. Two study areas are marked. The image represents the Landsat-7 ETM+ band 3 data acquired on May 21, 2000.

increases. Therefore, these mountain ranges receive more precipitation (Katznelson, 1957).

Observing the Landsat-7 image in Fig. 1, it is evident that the 200–300 mm isohyetal belt separates desert regions (such as the Negev and Judean deserts) from the non-desert parts of Israel with a sharp contrast. The non-desert regions are characterized by dark tones where different ground albedo features (such as cultivated fields, settlements, cities, etc.) can be recognized. In contrast, the other side of the belt is dominated by very bright tones, mostly totally white, and no details can be resolved. The sparse darker features are the relatively more humid mountains discussed above. Extensive bright areas can also be observed in the surrounding deserts such as the Sinai and the deserts in Jordan and Syria.

4. Data sets

Eight Landsat-7 scenes were examined in the current project (Table 2). As shown in Fig. 1, images of path 174 rows 37, 38, and 39 (according to the Worldwide Reference System 2 (WRS2)) correspond to three different climatic zones—sub-humid, semi-arid, and arid (respectively, from north to south). Two sets of these images were acquired on August 7, 1999 and May 21, 2000. Two single images, path/row = 174/39, were acquired on October 10, 1999 and August 27, 2001. The latter image was selected in order to determine if the changes in the spectral radiance range and the gain setting, applied by NASA on July 1, 2000 (NASA, WWW4), have improved the saturation phenomenon over the region.

Surface cover brightness is progressing from north to south across the rainfall isohyets as discussed above. The northern part of Israel (row 37) is characterized by pronounced darker tones than the southern part (row 39). Indeed, information provided by NASA (NASA, WWW5) indicates that images 174/38 and 174/39 are categorized as "Desert".

In addition, one Landsat-5 scene, path/row = 174/39, from September 21, 1995 was selected as a reference image (especially for the Landsat-7 174/39 image of October 10, 1999 due to the seasonal similarity). This image represents an end-of-summer image since we hypothesize that inter-annual variations are minimal after the long dry spell in the Negev Desert.

5. Analysis and results

5.1. Pre-processing

The images specified above were purchased from the US Geological Surveys (USGS) EROS Data Center (EDC). The Landsat-7 images were obtained as level 1G product (NASA, WWW4). Since the final product of this process was scaled to byte values, Eq. (2) is used for converting the DN into radiances (L_λ) (in $\mathrm{W\,m^{-2}\,ster^{-1}\,\mu m^{-1}}$) for each band ($\lambda$):

$$L_\lambda = L_{\min_\lambda} + \frac{L_{\max_\lambda} - L_{\min_\lambda}}{\mathrm{DN}_{\max} - \mathrm{DN}_{\min}} \times \mathrm{DN} - \mathrm{DN}_{\min} \quad (2)$$

where $L_{\min}$ and $L_{\max}$ are the spectral radiances for each band at $\mathrm{DN}_{\min} = 0$ and $\mathrm{DN}_{\max} = 255$, respectively.

Table 3 presents the gain states that were set according to the rules described previously. These gain states were obtained from the USGS web site (USGS, WWW6) along with the header information. The actual $L_{\min}$ and $L_{\max}$ values for these gain states, before and after July 1, 2000, were obtained from NASA (NASA, WWW4) and are presented in Table 4. It is important to note that, although the images were selected to represent different seasons, the sun elevations were higher than any of the thresholds indicated in Table 1. Nevertheless, it was found that in the Desert images (row 39) most of the bands were set to high

Table 2
Landsat-5 and Landsat-7 scenes involved in the current research with respect to their climatic zones

Satellite	Path/row	Climatic zone	Date of images			
Landsat-7	174/37	Sub-humid	August 7, 1999	–	May 21, 2000	–
Landsat-7	174/38	Semi-arid	August 7, 1999	–	May 21, 2000	–
Landsat-7	174/39	Arid	August 7, 1999	October 10, 1999	May 21, 2000	August 27, 2001
Landsat-5	174/39	Arid	–	September 21, 1995	–	–

Table 3
Gain settings (H = high, L = low) for the ETM+ images involved in the project along with the respective sun elevation angles (in degrees) (source: USGS, WWW5)

	August 7, 1999			October 10, 1999	May 21, 2000			July 27, 2001
	174/37 Sub-humid	174/38 Semi-arid	174/39 Arid	174/39 Arid	174/37 Sub-humid	174/38 Semi-arid	174/39 Arid	174/39 Arid
Band 1	H	H	H	H	H	H	H	L
Band 2	H	H	H	H	H	H	H	L
Band 3	H	H	H	H	H	H	H	L
Band 4	H	H	H	H	L	L	L	L
Band 5	H	H	H	H	H	H	L	L
Band 7	H	H	H	H	H	H	L	L
Sun elevation	62.1526	62.6416	63.066	48.1659	66.0291	66.4188	66.7281	63.5711

gain instead of low before July 1, 2001. After that date, the gain setting was revised and all bands were changed to low gain except for band 4 when the sun elevation is lower than 45°. Bearing in mind that scene 174/39 should be defined as Desert, it is assumed that wrong settings were selected in the images of August 7, 1999 and October 10, 1999 in all spectral bands as well as in bands 1, 2, and 3 of the image of May 21, 2000. The gain setting of the latest image in the current research, July 27, 2001, was set to low and hence is supposed to be correct for the desert area of Israel.

For atmospheric correction, aerosol optical thickness at 550 nm and total precipitable water data collected by a CIMEL sunphotometer at the Sede Boker AERONET site (Holben et al., 2001; Aeronet, WWW7), located at the center of the image 174/39, were introduced as input to the Second Simulation of the Satellite Signal in the Solar Spectrum (6S) code (Vermote et al., 1997). Corrections for molecular scattering, ozone, and the geometry of the sensor and the Sun were also applied. As a result, at-sensor radiances were converted into surface reflectances (ρ). All images were eventually co-registered to a master image of the area through a second-order transformation using the nearest neighbor resampling method. The precision of the results lies at the subpixel level. The Landsat-5 image, which had been obtained as raw data, was basically subjected to the same processing procedure except that the radiometric correction coefficients were chosen from Markham and Barker (1986).

5.2. Saturation recovery

After the above-described pre-processing and visual examination of the images, saturation can be observed on the earlier three row 39 images listed in Table 3, in terms of bright tones. Saturation occurs almost all

Table 4
ETM+ spectral radiance range for images acquired before and after July 1, 2000 (source: NASA, WWW4)

	Spectral radiance range ($W\,m^{-2}\,ster^{-1}\,\mu m^{-1}$)							
	Before July 1, 2000				After July 1, 2000			
	Low gain		High gain		Low gain		High gain	
	L_{min}	L_{max}	L_{min}	L_{max}	L_{min}	L_{max}	L_{min}	L_{max}
Band 1	−6.20	297.50	−6.20	194.30	−6.20	293.70	−6.20	191.60
Band 2	−6.00	303.40	−6.00	202.40	−6.40	300.90	−6.40	196.50
Band 3	−4.50	235.50	−4.50	158.60	−5.00	234.40	−5.00	152.90
Band 4	−4.50	235.50	−4.50	157.50	−5.10	241.10	−5.10	157.40
Band 5	−1.00	47.70	−1.00	31.76	−1.00	47.57	−1.00	31.06
Band 7	−0.35	16.60	−0.35	10.93	−0.35	16.54	−0.35	10.80

over the image except at the high mountain ranges. Frequency histograms of the reflectances for these images are presented in Fig. 2A–C. From these figures it is apparent that image saturation exists in bands 2, 3, 4, 5, and 7 on August 7, 1999; in bands 3 and 5 on October 10, 1999; and in bands 2 and 3 on May 21, 2000. No such significant saturation exists on August 27, 2001, except for a few pixels in bands 3 and 5 (Fig. 2D) and no saturation exists in the Landsat-5 image.

For further investigation of the saturation phenomenon, two different studies were conducted based

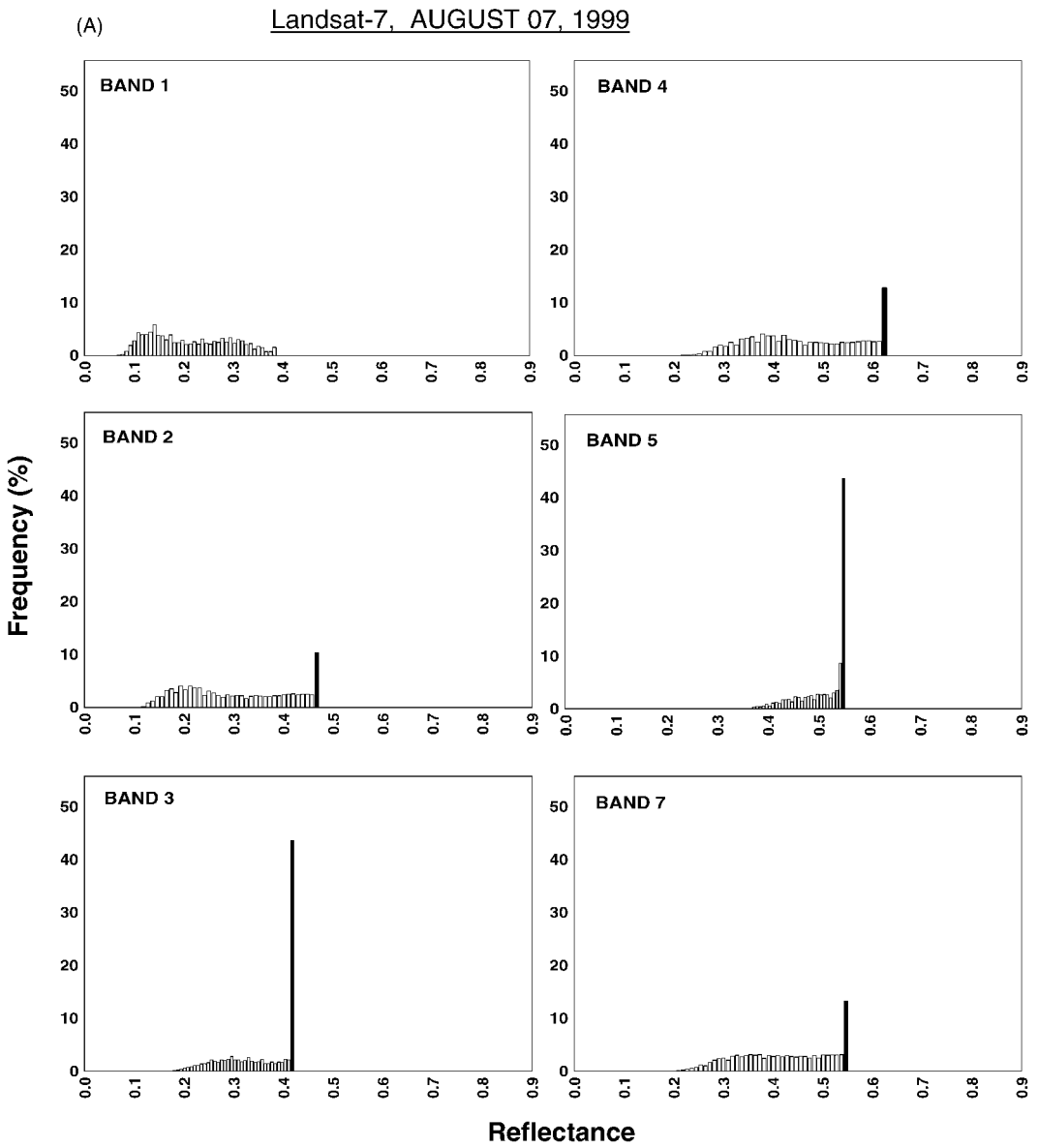

Fig. 2. Reflectance histograms of the four path/row = 174/39 images involved in the current research. Note the saturation in different spectral bands (solid bars). (A) August 7, 1999; (B) October 10, 1999; (C) May 21, 2000; (D) August 27, 2001. Data obtained from the study area #2 shown in Fig. 1.

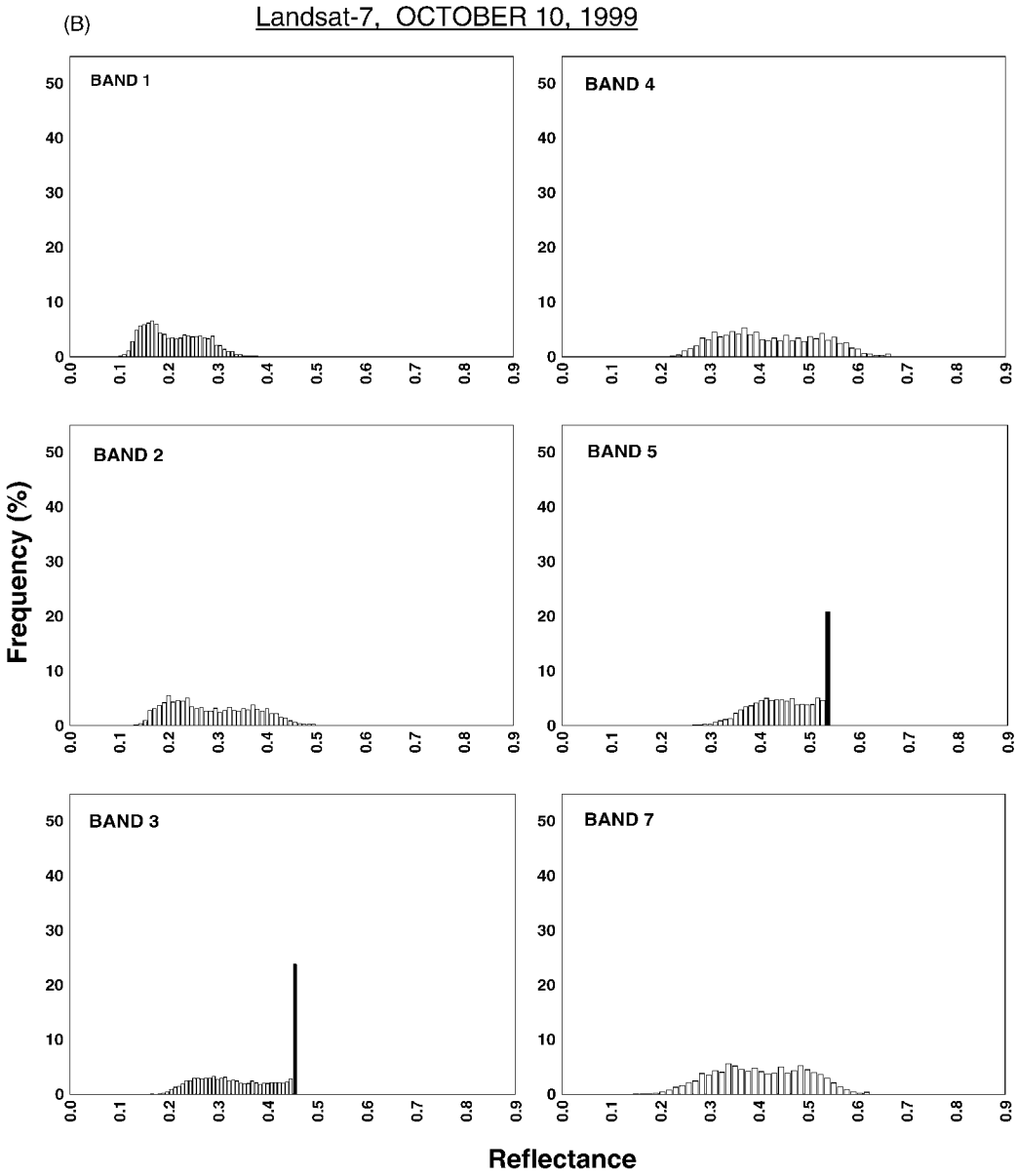

Fig. 2. (*Continued*)

on earlier studies (e.g., Price, 1995; Karnieli et al., 2001) that found high correlations among spectral bands for a similar ground feature (e.g., soil, vegetation, or water). Since desert landscape is usually composed of relative homogeneous coverage (mostly bare soils or rocks with scare amount of vegetation) it is expected that correlation does exist in the hyper spectral domain and maybe also exists in the ETM+ multi spectral domain. In order to examine this hypothesis, a preliminary investigation was conducted in the hyper arid region of southern Israel (Fig. 1, denoted as study area #1). Fig. 3A presents library spectra (USGS, WWW8) of the six most common minerals of the area (Hematite, Goethite,

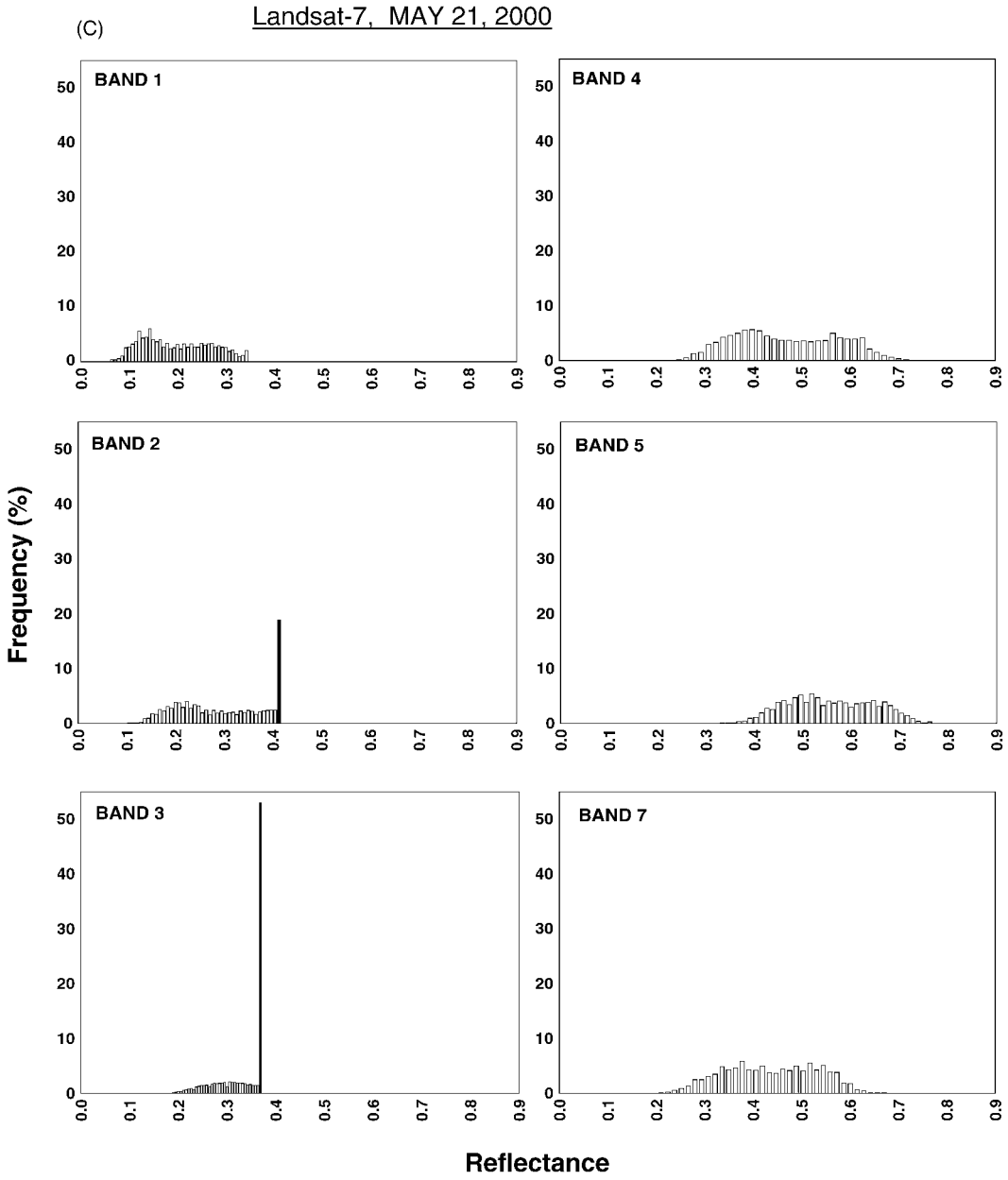

Fig. 2. (*Continued*)

Dolomite, Quartz, Kaolinite, and Gypsum) while Fig. 4A presents spectra of several arid surfaces (dune sand, loess, reg, and alluvium) as were measured in situ with the Analytical Spectral Devices (ASD) field spectrometer. These spectra were re-sampled into the six ETM+ spectral bands using the spectral response function of each band (Figs. 3B and 4B). From both figures it can be seen that although specific information was lost during the re-sampling, basic spectral trends maintain constant. In order to statistically

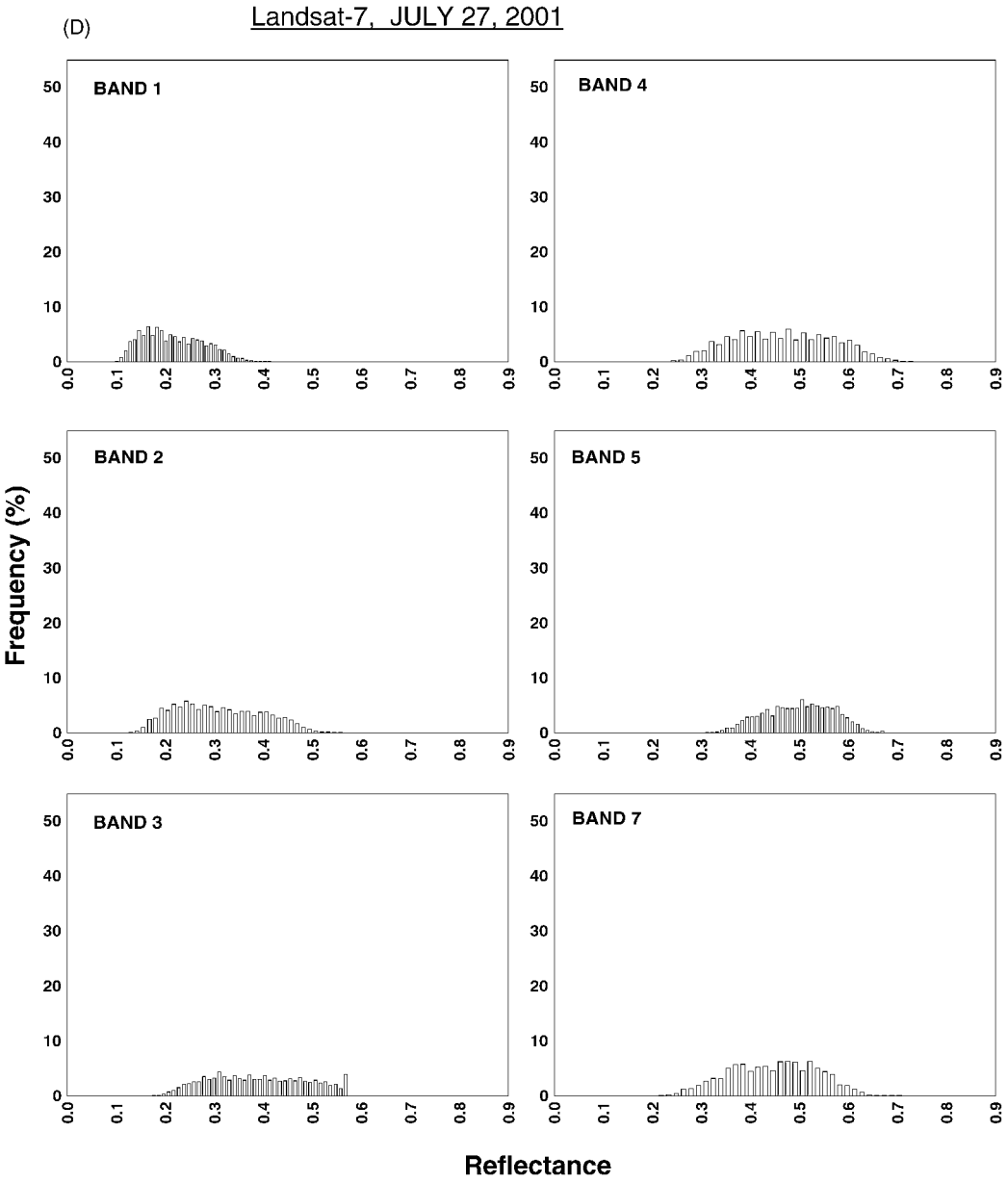

Fig. 2. (*Continued*).

examine the above assumption about the tight relationships between the spectral bands, multivariate correlation analysis among all simulated ETM+ spectral bands was applied and the results are summarized in Table 5. Also given in Table 5 the results of the correlation between the simulated reflectances and different band manipulations. Table 5 reveals a relatively good correlation among all bands, whereas the highest correlation values were obtained between the simulated reflectances and regression within a multiple combination of bands 2, 4, and 7. As discussed earlier, these results strongly strengthen the idea that

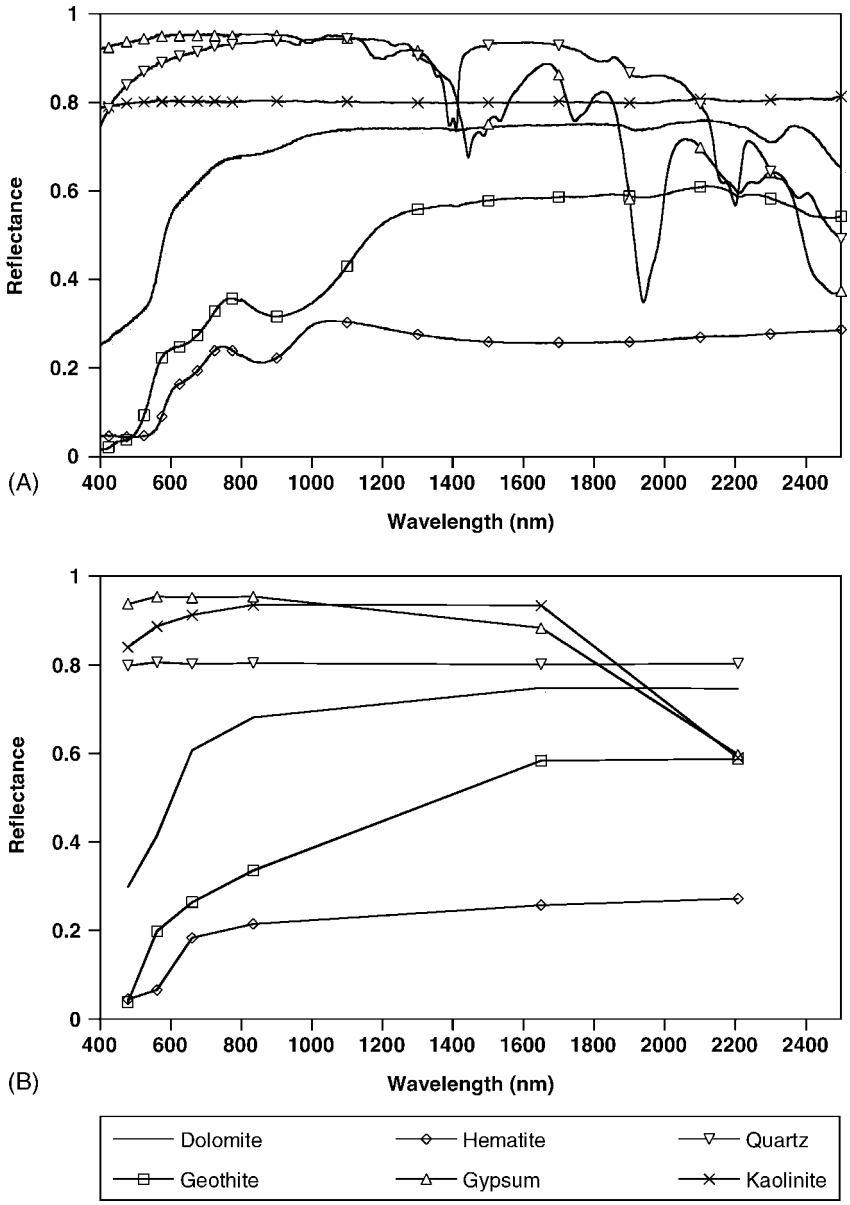

Fig. 3. (A) Library spectra of the six most common minerals of the study area, Hematite, Goethite, Dolomite, Kaolinite, Quartz, Gypsum (source: USGS, WWW8). (B) The same spectra resampled into the six ETM+ spectral bands using the spectral response function of each band.

regression between the spectral bands may be used as a correction technique for real ETM+ data.

Bearing in mind the previous results, the next step was to perform similar analytical procedure to a set of appropriate ETM+ data. This was implemented and demonstrated on the image of May 21, 2000; path/row = 174/39, where saturation affects bands 2 and 3. Fig. 5A and B shows the distribution of the saturated pixels of bands 2 and 3 within the scene. For this purpose reflectances were extracted from the same image along a sampling area in each of the row 39 images, a total of 15 480 pixels (Fig. 1, denoted as study area

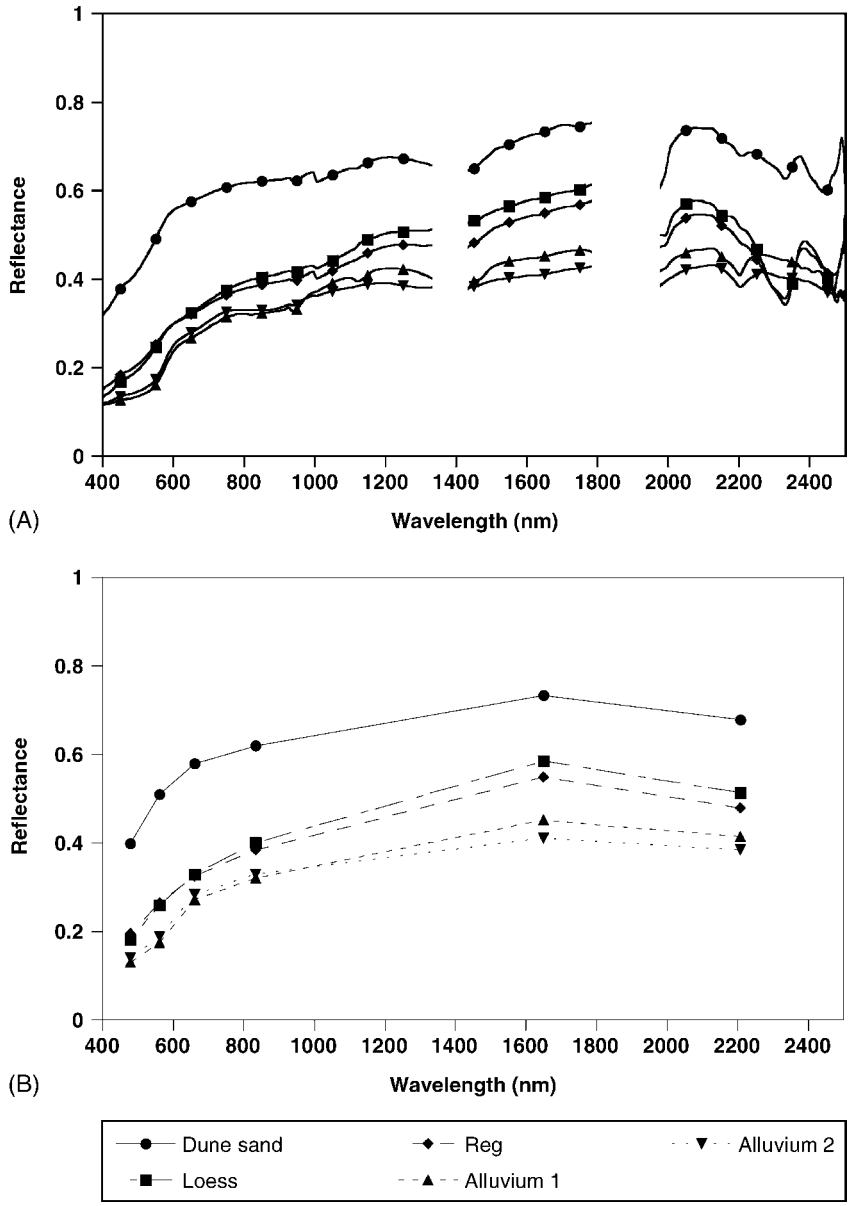

Fig. 4. (A) Spectra of several arid surfaces as were measured in situ in the study area. (B) The same spectra re-sampled into the six ETM+ spectral bands using the spectral response function of each band.

#2). This sampling area, about 80 km long, covers both relatively bright and relatively dark pixels. Profiles of reflectances along the sampling area (Fig. 6) show the difference between the high values over the bright part versus the lower values over the darker part. The saturation of band 3, characterized by plateaus at reflectance level of 38% can be recognized in the bright part along the sampling area.

A statistical procedure is suggested for overcoming the saturation problem in the reflective bands of the ETM+ based on the correlation hypothesis demonstrated above. However, this correlation becomes

Table 5
Correlation matrix (r^2) among reflectances resulted from simulated ETM+ spectral bands as well as results of correlation between the simulated reflectances and different band manipulations

	Band 1	Band 2	Band 3	Band 4	Band 5	Band 7
Band 1	1.00					
Band 2	0.97	1.00				
Band 3	0.96	0.99	1.00			
Band 4	0.94	0.98	0.99	1.00		
Band 5	0.86	0.92	0.94	0.96	1.00	
Band 7	0.82	0.88	0.90	0.90	0.95	1.00
(Band 1 + band 7)/2	0.92	0.96	0.96	0.95	0.96	0.98
(Band 1 + band 5)/2	0.93	0.97	0.98	0.98	0.99	0.94
(Band 2 + band 5)/2	0.92	0.98	0.98	0.99	0.99	0.94
Reg (band 1, band 2, band 7)	0.96	1.00	1.00	0.98	0.93	0.90

worse when saturation occurs. In order to test this suggestion, a multivariate correlation analysis was performed on the Landsat-5 image of the Negev (path/row = 174/39). Table 6A presents the statistical results that confirm the hypothesis. However, similar multivariate correlation analysis, performed on the Landsat-7 image of May 21, 2000, reveals lower correlations between the saturated band 3 and the other spectral bands (Table 6B).

The following section is aimed at proposing a procedure for reconstructing saturated bands by using the reflectances of their unsaturated parts along with those of the other unsaturated bands. In the first stage bands 3 (saturated) and 4 (unsaturated) of the May 21, 2000 row 39 image are used as an example. The following steps are proposed for achieving the close-to-reality recovery:

(1) start by observing the saturation on the image histogram as shown in Fig. 2C;
(2) present the scatterplot of the saturated band as a function of another, unsaturated, band (Fig. 7A). In the present data set the saturation part of band 3 can be seen when the reflectance points are concentrated along a horizontal line rather than along the expected continuous correlation line;

Table 6
Correlation matrix (r^2) among reflectances of the reflective spectral bands (A) Landsat-5, path/row = 174/39, September 21,1995; (B) Landsat-7, path/row = 174/39, May 21, 2000

	Band 1	Band 2	Band 3	Band 4	Band 5	Band 7
(A) Landsat-5						
Band 1	1.00					
Band 2	0.98	1.00				
Band 3	0.96	1.00	1.00			
Band 4	0.92	0.98	0.98	1.00		
Band 5	0.85	0.88	0.90	0.90	1.00	
Band 7	0.86	0.88	0.88	0.88	0.94	1.00
(B) Landsat-7						
Band 1	1.00					
Band 2	0.92	1.00				
Band 3	0.45	0.58	1.00			
Band 4	0.91	0.92	0.53	1.00		
Band 5	0.83	0.83	0.49	0.91	1.00	
Band 7	0.78	0.79	0.45	0.80	0.89	1.00

Note the extremely low correlation coefficients associated with Landsat-7 band 3.

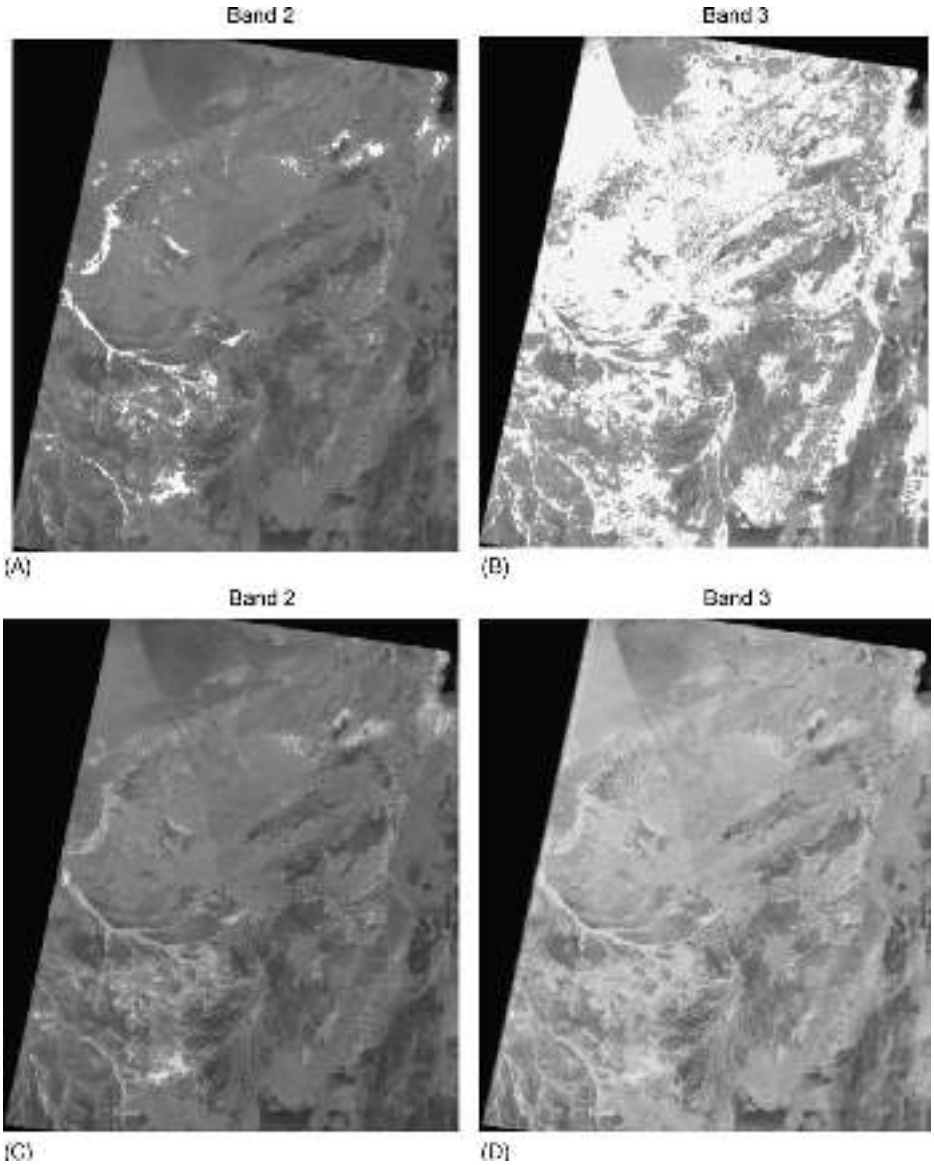

Fig. 5. Selected bands of the May 21, 2000 image. (A) Band 2, with saturated pixels; (B) Band 3, with saturated pixels; (C) Band 2, after saturation correction; (D) Band 3, after saturation correction.

(3) eliminate the pixels within the saturation zone from the data set and calculate the regression parameters (Fig. 7B);
(4) perform extrapolation, based on the new linear regression parameters, for relocating the eliminated pixels along the extension of the regression line (Fig. 7C); and
(5) apply the correction equation on a pixel-by-pixel basis on the entire image, and thus recovering the values of the saturated pixels.

For more accurate results, it is proposed that all bands be involved in the process, using a multiple regression analysis. In the multivariate case, the linear

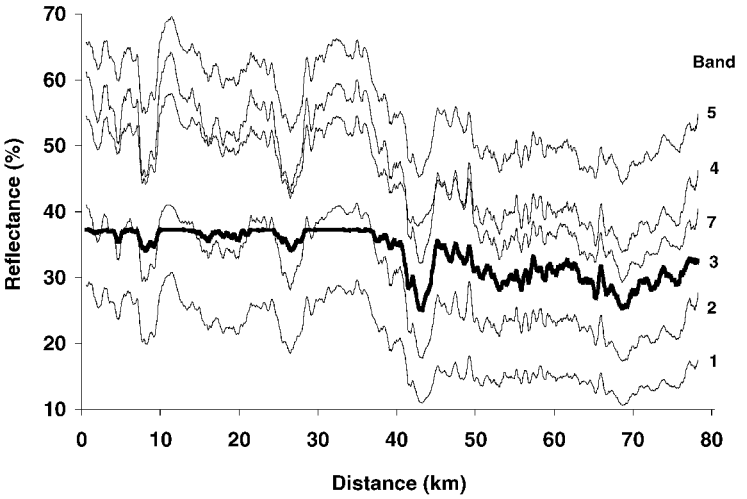

Fig. 6. Profiles of reflectances along the study area #2 marked on Fig. 1 for the May 21, 2000 image. Note the saturation of the band 3 profile (in bold) expressed as the long plateaus over the brighter area.

equation contains the reflectances of the saturated band (ρ_s) as a dependent variable and the reflectances of the remaining five ETM+ bands (ρ_n) as independent variables. The linear multiple regression equation has the form:

$$\rho_s = a + b_1\rho_1 + b_2\rho_2 + \cdots + b_n\rho_n \quad (3)$$

where $\rho_1, \ldots, \rho_n$ are the reflectances of the n unsaturated bands, and a and $b_1, \ldots, b_n$ are the multiple regression parameters. Results of the multivariate regression analysis for bands 2 and 3 of the May 21, 2000 image are demonstrated in Fig. 5C and D. The difference in sharpness and in observed details are remarkable. It is important to note that the regression parameters for correcting any given data set must be performed for the data in question and cannot be transferred from one data set to another. This is basically due to the fact that different atmospheric correction

Table 7
Comparison of the information content of data from Landsat-5 TM and Landsat-7 ETM+ over the desert environment, in terms of entropy

		Band 1	Band 2	Band 3	Band 4	Band 5	Band 7	Total
(A) Entropy (bit/pixel)								
Landsat-5	September 21, 1995	6.754	6.316	6.802	6.624	7.028	6.564	40.089
Landsat-7	August 7, 1999	6.803	6.992	5.592	6.955	5.304	7.042	38.688
Landsat-7	October 10, 1999	6.737	7.136	6.494	7.129	6.563	7.183	41.243
Landsat-7	May 21, 2000	6.892	6.458	4.152	6.811	6.808	6.880	38.001
Landsat-7	August 27, 2001	6.570	6.988	7.252	6.889	6.823	6.855	41.378
Landast-7[a]	May 21, 2000	6.892	7.299	7.137	6.811	6.808	6.881	41.828
(B) Entropy differences (bit/pixel)								
Landsat-7	August 7, 1999	0.049	0.675	−1.210	0.331	−1.724	0.477	−1.401
Landsat-7	October 10, 1999	−0.018	0.820	−0.308	0.505	−0.465	0.619	1.153
Landsat-7	May 21, 2000	0.138	0.141	−2.651	0.187	−0.220	0.315	−2.088
Landsat-7	August 27, 2001	−0.184	0.672	0.450	0.265	−0.205	0.291	1.288
Landast-7[a]	May 21, 2000	0.138	0.982	0.335	0.187	−0.220	0.316	1.739

(A) Entropy values (bits/pixel); (B) difference in information content between the different ETM+ scenes and the TM.
[a] Results after the saturation correction that was applied on bands 2 and 3.

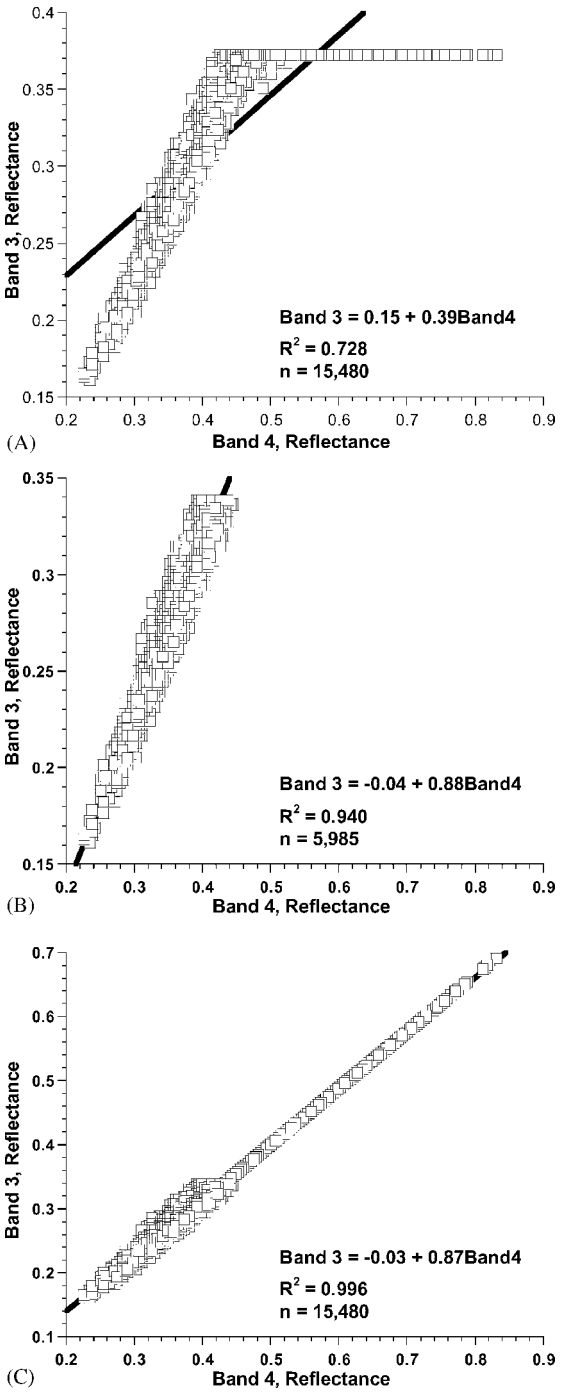

techniques can be used by different users, different illumination conditions may be introduced in different data sets, area coverage may be differ from one season to another, and different sensor sensitivity may be obtained in different duration. This leads to the conclusion that the correction factors are scene-data dependent and strictly need to be extracted from a specific set.

5.3. Entropy analysis

Results of the entropy analysis for the Landsat-5 TM and Landsat-7 ETM+ spectral bands, for different acquisition dates, are presented in Fig. 8 and Table 7A. Data obtained from the study area #2 represent the hyper-arid zone of the Negev and are characterized by relatively bright tones (Fig. 1) due to the saturation phenomenon as discussed earlier. Table 7B shows the difference in information content between the Landsat-7 data sets and those of the Landsat-5 used as reference. In all Landsat-7 images, band 1 has similar information content as Landsat-5. Band 2 exhibits a greater information content (0.67–0.82 bits/pixel) relative to the Landsat-5 TM sensor except for the May 21, 2000 image when it was saturated. Band 3 suffered from saturation on all dates prior to July 1, 2000 and therefore shows less information content on those days relative to the TM sensor. On the image of August 27, 2001 entropy of band 3 shows increased information content of 0.45 bits/pixel. Band 4 in all four images has a relatively small increase in information content of 0.2–0.5 bits/pixel. Band 5, in all Landsat-7 images, shows a worse performance than Landsat-5 of 0.2–1.7 bits/pixel. Even the gain setting change, from high to low, on the latest two images did not improve this situation. Finally, band 7 reveals a stable improvement compared to the TM sensor of about 0.2–0.6 bits/pixel.

Fig. 7. An example of the statistical procedure for recovering a saturated band. (A) Scatterplot of band 3 vs. band 4. The saturation part of band 3 is obvious where the reflectance points are concentrated along a horizontal line rather than the expected inclined correlation line. (B) The same relationships without the saturated points. A new regression equation is calculated. (C) Correction of the saturated pixels by extrapolation along the extension of the regression line.

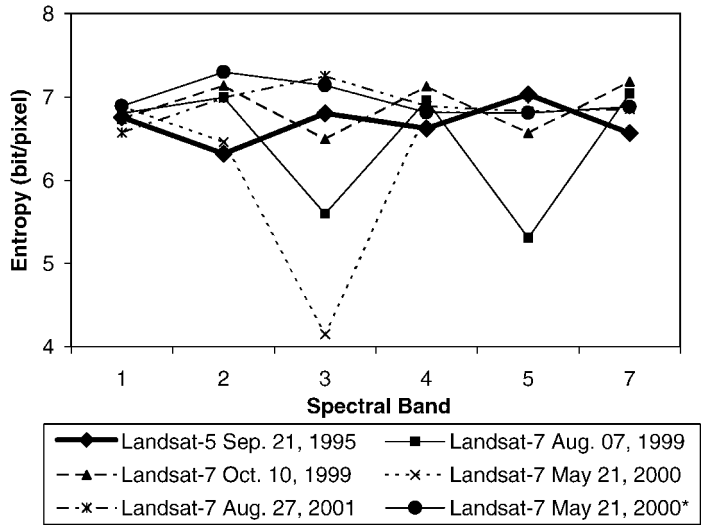

Fig. 8. Entropy analysis for Landsat-7 ETM+ spectral bands of different acquisition dates in comparison to those of Landsat-5 TM. Data obtained from the study area #2 are shown in Fig. 1. Note that the line for May 21, 2000 that is marked with * was created after the saturation correction that had been applied on bands 2 and 3.

The total image entropy values of the Landsat-7 data sets produced mixed results compared to those of Landsat-5 (Table 7). However, it can be seen that the latest image (August 27, 2001) has higher values than Landsat-5. It is important to point out the improvement in the results after applying the proposed saturation correction procedure. The problematic bands 2 and 3 exhibited an increased information content of 0.8 and 3.0 bits/pixel, respectively.

6. Discussion

The radiometric calibration of Landsat-7 ETM+ is supposed to have less uncertainty than that of the Landsat-5 TM (Markham, personal communication). The two-gain states along with the six Earth surface categories constitute significant improvements in the Landsat-7 ETM+ sensor over the TM. They are believed to provide the user with more radiometric precision and consequently with the ability to achieve better results with land-use and land-cover characterization for fulfilling the mission goals.

This paper highlights the reliability of the Landsat-7 ETM+ absolute calibration and the gain setting. Since no other saturation difficulties have been evidenced from other parts of the world and the vicarious calibration campaigns have generally revealed positive results, apparently, the saturation problem exists mainly along the desert transition zones where part of the scene can be defined as "land" while the other as "desert" as in the case of the images over Israel. The early Landsat-7 images over the region show no consistency in the saturated bands and no consistency in the saturation locations associated with the reflectances. The proposed statistically based procedure provides a reasonable solution for any saturated band.

It is currently believed that radiometric saturation difficulties occurred only during the first year of operation. These are probably the result of using the pre-launch calibration. About a year after operation, the revision of the spectral radiance range (L_{min}'s or L_{max}'s values) and a new gain setting were announced at NASA's web site. Normally, there is no need to change these values unless something drastic happens on the instrument or the sensitivity of the instrument increases, which is not expected. If the sensitivity decreases, the L_{max} values can be increased, and by so doing, the usable dynamic range of the product is increased. The changes that have taken place after a year of operation are mostly due to the adoption of the "improved" pre-launch gains for the instrument that

have, in effect, "increased" its sensitivity (Markham, personal communication).

Calculations of the entropy analysis are generally similar to those presented by Masek et al. (2001), however the following differences can be counted: (1) these authors sampled seven of the most typical land-cover categories but desert; (2) they did not apply atmospheric correction before the entropy analysis; (3) they used an ETM+ image of July 28, 1999 that was acquired in high gain mode.

The current results, prior to July 1, 2000, do not completely agree with those of Masek et al. (2001). This is mainly due to the saturation phenomenon that influences the performance of bands 3 and 5. If we accept the assumption that the change in band setting from high to low gain along with the change of the spectral radiance range after July 1, 2000 have led to a better performance of the ETM+ sensor, from the entropy analysis, it is evident that there has been an improvement of between 0.26 and 0.67 bits in bands 2, 3, 4, and 7, but a slight decrease in information content (about 0.2 bits) in bands 1 and 5. However, this research, over the desert environment, has never reached 1 bit of extra data as noted by Masek et al. (2001).

7. Summary

The currently implemented gain setting strategy for Landsat-7 ETM+ consists of a fixed categorization of the earth's surface cover types. Gain setting rules, which are based on surface cover and sun angle, are aimed at improving the interpretation of land-use and land-cover in the changing environment. However, efforts to analyze these images over the Negev Desert of Israel show that the detectors are subject to saturation. This phenomenon occurred at least during the first year of operation. Revisions in the spectral radiance range and the gain setting, implemented on July 1, 2000, seem to have reduced the saturation phenomenon over the region, but this still needs to be tested on more images. Nevertheless, a statistically based procedure is proposed in order to overcome the difficulties and to improve the saturated scenes. Reflectance values of saturated pixels can be replaced by close-to-reality values, based on the hypothesis that high correlation exists between the different spectral bands. The current proposed method can be applied for other climatic regions, such as scenes partially covered by snow, and other multi- and hyper-spectral sensors.

Acknowledgements

The authors would like to thank Dr. Yoram Kaufman (NASA/GSFC) for his important comments and Dr. Charles Ichoku (NASA/GSFC) for editing the manuscript. This research is partially supported by the Survey of Israel.

Appendix A. URL address

WWW1: http://earthobservatory.nasa.gov/Library/Landsat/landsat5.html,
WWW2: http://www.ccrs.nrcan.gc.ca/ccrs/learn/terms/glossary/glossary_e.html,
WWW3: http://ltpwww.gsfc.nasa.gov/IAS/handbook/handbook_htmls/chapter6/chapter6.html,
WWW4: http://ltpwww.gsfc.nasa.gov/IAS/handbook/handbook_htmls/chapter11/chapter11.html,
WWW5: http://ltpwww.gsfc.nasa.gov/IAS/ascii/desert.lst,
WWW6: http://edcimswww.cr.usgs.gov/pub/imswelcome/,
WWW7: http://aeronet.gsfc.nasa.gov,
WWW8: http://speclab.cr.usgs.gov/spectral-lib.html.

References

Goward, S.N., Masek, J.G., Williams, D.L., Irons, J.R., Thompson, R.J., 2001. The Landsat 7 mission—terrestrial research and applications for the 21st Century. Remote Sensing Environ. 78, 3–12.

Holben, B.H., Tanre, D., Smirnov, A., Eck, T.F., Slutsker, I., Chatenet, B., Lavenue, F., Kaufman, Y.J., Van De Castle, J., Setzer, A., Markham, B., Clark, M., Frouin, R., Karnieli, A., O'Neill, N., Pietras, C., Pinker, R., Voss, K., Zibordi, G., 2001. An emerging ground based aerosol climatology: aerosol optical depth from AERONET. J. Geophys. Res. 106 (12), 12067–12097.

Karnieli, A., Kaufman, Y.J., Remer, L.A., Ward, A., 2001. AFRI—aerosol free vegetation index. Remote Sensing Environ. 77, 10–21.

Katznelson, J., 1957. The climate of the Negev. Teva Vaaretz 1, 310–318.

Malila, W.A., 1985. Comparison of the information contents of Landsat TM and MSS data. Photogrammetric Eng. Remote Sensing 51, 1449–1457.

Markham, B.L., Barker, J.L., 1986. Landsat-MSS and TM Post Calibration Dynamic Ranges, Atmospheric Reflectance and At-Satellite Temperature. Earth Observation Satellite Company, Lanham, MD, USA.

Masek, J.G., Honzak, M., Goward, S.N., Liu, P., Pak, E., 2001. Landsat-7 ETM+ as an observatory for land cover—initial radiometric and geometric comparisons with Landsat-5 Thematic Mapper. Remote Sensing Environ. 78, 118–130.

Price, J.C., 1984. Comparison of the information content of data from the Landsat-4 Thematic Mapper and the multispectral scanner. IEEE Trans. Geosci. Remote Sensing 22, 272–281.

Price, J.C., 1995. Examples of high resolution visible to near-infrared reflectance spectra and a standardized collection for remote sensing studies. Int. J. Remote Sensing 16, 993–1000.

Shannon, C.E., 1948. A mathematical theory of communication. Bell Syst. Tech. J. 27, 379–423, and 623–656.

Sofer, A., 1979. The Negev—a geographical definition. In: A. Shmueli & Y. Gradus (Eds.), The Land of the Negev—Man and Desert. Publishing House, Ministry of Defence, Tel Aviv, pp. 3–8.

Teillet, P.M., Barker, J.L., Markham, B.L., Irish, R.R., Fedosejevs, G., Storey, J.C., 2001. Radiometric cross-calibration of the Landsat-7 ETM+ and Landsat-5 TM sensors based on tandem data sets. Remote Sensing Environ. 78, 39–54.

Thome, K., Markham, B., Barker, J., Slater, P., Biggar, S., 1997. Radiometric calibration of Landsat. Photogrammetric Eng. Remote Sensing 63, 853–858.

Thome, K.J., 2001. Absolute radiometric calibration of Landsat 7 ETM+ using the reflectance-based method. Remote Sensing Environ. 78, 27–38.

Vermote, E., Tanré, D., Deuzé, J.L., Herman, M., Morcrette, J.J., 1997. Second Simulation of the Satellite Signal in the Solar Spectrum (6S): an overview. IEEE Trans. Geosci. Remote Sensing 35, 675–685.

Vogelmann, J.E., Helder, D., Morfitt, R., Choate, M.J., Merchant, J.W., Bulley, H., 2001. Effects of Landsat 5 Thematic Mapper and Landsat 7 Enhanced Thematic Mapper Plus radiometric and geometric calibrations and corrections on landscape characterization. Remote Sensing Environ. 78, 55–70.